Tectonophysics 646 (2015) 106–116

Contents lists available at ScienceDirect

Tectonophysics

journal homepage: www.elsevier.com/locate/tecto

Crustal structure of the Pannonian Basin: The AlCaPa and Tisza Terrains and the Mid-Hungarian Zone

György Hetényi [a,b,*], Yong Ren [c,1], Ben Dando [c,2], Graham W. Stuart [c], Endre Hegedűs [d], Attila Csaba Kovács [d], Gregory A. Houseman [c]

[a] Swiss Seismological Service, ETH Zürich, Zürich, Switzerland
[b] Department of Earth Sciences, ETH Zürich, Zürich, Switzerland
[c] School of Earth and Environment, University of Leeds, Leeds LS2 9JT, UK
[d] Geological and Geophysical Institute of Hungary, Budapest, Hungary

ARTICLE INFO

Article history:
Received 10 October 2014
Received in revised form 3 February 2015
Accepted 6 February 2015
Available online 19 February 2015

Keywords:
Geodynamics
Crust
Pannonian Basin
Extension
Converted waves
Gravity

ABSTRACT

The Pannonian Basin of Central Europe is one of the key examples of Miocene continental extension that is easily accessible to surface seismological investigation. It comprises two major crustal blocks: AlCaPa and Tisza which abut along a poorly understood structure referred to as the Mid-Hungarian Zone (MHZ), the whole being surrounded by the arc of the Carpathian Mountains, the Alps and the Dinarides. Using data from the CBP (Carpathian Basins Project) temporary broadband seismic array of 46 stations deployed across the western Pannonian Basin in 2006–2007, we calculated receiver functions that constrain the variation of crustal thickness across the basin and derive a map of Moho depth across a NW–SE oriented swath about 450 km long and 75 km wide. The measured Moho depths show no significant change in crustal thickness between AlCaPa and Tisza terrains, but the Moho is not or very weakly imaged along a ca. 40 km wide strip centred on the MHZ. Moho depths within the Pannonian Basin are typically in the range 25–30 km, and increase toward the periphery of the basin. Our measurements are generally consistent with earlier V_P models from controlled-source seismic surveys and recent V_S models determined by tomographic analysis of ambient noise signals. The lack of a sharp Moho image beneath the MHZ suggests that the crust–mantle boundary in that zone may consist of a gradual increase in velocity with depth. The relatively constant crustal thickness across the two domains of the Pannonian Basin suggests that thinning to the same final state is controlled thermally. This structural characteristic seems to be governed by a large-scale balance of gravitational potential energy that is insensitive to the separate prior histories of the two regions.

1. Introduction and geodynamic setting

The Pannonian Basin is a major extensional basin within the southern part of the European continent. It has undergone multiple phases of tectonic activity through most of the Cenozoic, culminating in an episode of rapid lithospheric extension and contemporaneous shortening in the surrounding Carpathians during the mid-Miocene (~17.5–10.5 Ma), followed by late-Miocene to recent (~10.5–0 Ma) thermal subsidence and minor convergent reactivation (NE–SW) since ca. 5 Ma (Csontos et al., 1992; Horváth, 1993; Horváth et al., 1988, 2006; Tari et al., 1999). Since the Pliocene there is clear evidence of minor NE–SW contraction which is attributed to the renewed convergence of Adria and Europe, as summarised by Cloetingh et al. (2006). The Pannonian basement is comprised of two distinct terrains of different provenance: AlCaPa (Alpine–Carpathian–Pannonian) and Tisza–Dacia occupying respectively the northwest and southeast parts of the basin, each extending as far as the surrounding Carpathian Mountains (Fig. 1). In this paper we focus on the western part of the Pannonian basin using data from AlCaPa and Tisza blocks only. Stegena et al. (1975) referred to Gondwanan and European origins respectively for these two terrains, and more recent authors acknowledge these affinities. Csontos and Nagymarosy (1998) described the Palaeozoic and Mesozoic sequences of the AlCaPa terrain being similar to those of the Southern Alps, while high-grade crystalline rocks and late Variscan granites underlie the basement to the Tisza terrain. Tari et al. (1999) describe an alternation of unmetamorphosed Permo-Mesozoic units with Hercynian crystalline rocks in the Tisza Terrain produced by Cretaceous thrust faulting later dissected by Miocene extensional features.

Csontos and Vörös (2004) emphasised the distinct provenance of all the intra-Carpathian units derived from different Mesozoic tectonic units. Schmid et al. (2008) also described the separate European origins of the Dacia and Tisza blocks (derived from earlier rifting episodes) and

* Corresponding author at: Sonneggstrasse 5, 8092 Zürich, Switzerland.
E-mail address: gyorgy.hetenyi@sed.ethz.ch (G. Hetényi).
[1] Now at: GX Technology EAME Ltd., 1st Floor, Integra House, Vicarage Road, Egham TW20 9JZ, UK.
[2] Now at: Pinnacle, a Halliburton service, Unit 4A, Wheal Kitty Workshops, St. Agnes, Cornwall TR5 0RD, UK.

http://dx.doi.org/10.1016/j.tecto.2015.02.004
0040-1951/

an Adrian provenance for the AlCaPa block. Sea-floor spreading has been interpreted along several branches of the Neo-Tethys, including the Meliata–Vardar–Mures ocean, by Csontos and Vörös (2004). This ocean, which in closing produced the Vardar ophiolites in late Jurassic or early Cretaceous times, represents the major divide between the Dinarides of Adrian provenance from the other intra-Carpathian tectonic units by then assembled further to the north-east (Schmid et al., 2008). The suture of the Vardar Ocean corresponds to the present-day locus of the Paleogene to early Miocene magmatic belt (Kovács et al., 2007) that extends eastward from the Dinarides to Fruska Gora (FGS on Fig. 1).

The AlCaPa and Tisza terrains abut along an imprecisely defined ENE-striking structure known as the Mid-Hungarian Zone (MHZ) that is clearly delineated in the free-air gravity field (Fig. 1). This somewhat enigmatic structure has been interpreted in various ways: Csontos and Nagymarosy (1998), using evidence from seismic exploration lines, interpreted the Mid-Hungarian Fault (which bounds the MHZ to the south, Fig. 1) basically as a north-dipping detachment fault, reactivated from a previously south-vergent thrust fault, noting also the evidence for recent sinistral wrenching. Ustaszewski et al. (2008) interpreted that the MHZ originated as a transfer structure separating southward subduction of Europe beneath the Alps from northward subduction of the Adriatic plate beneath the Dinarides. Tectonic reconstructions for the region usually imply, however, that substantial dextral wrenching occurred along the MHZ as the Tisza terrain was extruded into the Carpathian embayment more slowly than the AlCaPa terrain (Csontos et al., 1992). Tari et al. (1999) suggest that up to 300 km of strike-slip displacement may have occurred along the Mid-Hungarian shear zone. The observation that the MHZ is near parallel to the main direction of extension in the basin, as interpreted for example by Ustaszewski et al. (2008), supports the idea that it is essentially a strike-slip feature, though estimated extensional displacements of up to ca. 180 km suggest that much if not most of the inferred 300 km of strike-slip displacement must have preceded the main phase of Miocene extension.

Both terrains have undergone significant rotation since the early Miocene, the AlCaPa counterclockwise and the Tisza clockwise, as recorded by paleomagnetic declination and apparent rotation of the principal stress directions (Csontos et al., 1991, 1992; Patrascu et al., 1994). Although the movements of these tectonic terrains are often referred to as block-like or plate-like, it is likely that both terrains have undergone an extensive penetrative deformation in order to produce the present configuration (Csontos et al., 2002). Lorinczi and Houseman (2010) constructed continuum deformation models based on a viscous constitutive law that could explain some of the characteristics of the observed deformation, including the NE translation, lithospheric extension and spatially variable rotation. In general, those models require convergence perpendicular to the present MHZ. They also assume that the observed deformation field is produced by a combination of boundary stresses due to a retreating Carpathian boundary (as described by Horváth, 1993) and extensional collapse of an over-thickened Alpine orogenic wedge (as discussed by Horváth et al., 2006). An indenting Adriatic plate created an initial condition of high topography in the Alps and Dinarides, after which internal buoyancy forces played the major role in producing synchronous extension in the basin and convergence in the Carpathians (Gemmer and Houseman, 2007). The idea that Pannonian lithosphere prior to extension formed a convergent mountain belt similar to and probably contiguous with the Eastern Alps was proposed by Dando et al. (2011) in order to explain relatively high seismic velocities at mid-upper mantle depths in a band stretching across the present-day Pannonian Basin.

Tari et al. (1999) summarised an extensive catalogue of geological and geophysical data that constrain the structure of the crust in the Pannonian Basin. They interpret an initial extensional collapse phase at the beginning of the Mid-Miocene characterized by metamorphic core complex formation. The collapse phase was followed by a broadly distributed phase of upper-crustal faulting that affected most of the basin but eventually gave way to a failed rift in the SE Pannonian (with greatest extension producing the Makó and Békés basins). Posgay et al. (2006) described extensive evidence from core and seismic properties of retrograde metamorphism that has occurred as shallow basement was uplifted from mid-crustal levels during basin extension. Following on from early subsidence analyses by Sclater et al. (1980), Horváth et al. (1988), Tari et al. (1992, 1999) show that extension factors are spatially variable and, in general, lithospheric thinning factors (ca. 2 to 3) are much greater than the corresponding crustal thinning factors (ca. 1.5 to 2) in order to explain the observed thermal subsidence. Transect C of Tari et al. (1999) is particularly relevant to the present investigation and emphasises a ca. 160 km offset to the NW of the most highly strained upper crust relative to the location of maximum lithospheric thinning. They note in accounting for the asymmetry that a large strike-slip offset along the MHZ may have juxtaposed different lithospheric/crustal structures. Their reconstructions emphasise the 3-dimensional nature of the extensional strain field under a principal extension direction that is NE, near parallel to the strike of the MHZ.

Earlier seismic investigations of the Pannonian Basin crust have relied largely on controlled source experiments (as summarised by Tari et al., 1999 and Grad et al., 2009). These data have provided important insights into the structure of the upper crust and the overall thickness and seismic velocity distribution within individual crustal sections (e.g. Grad et al., 2006). More recently, the analysis of ambient seismic noise from a basin-wide array of broad-band seismic recorders has enabled the application of tomographic techniques to determine a new high-resolution crustal velocity model for the entire region (Ren et al., 2013). This model is in broad agreement with prior compilations of controlled source data (Grad et al., 2009; Tesauro et al., 2008) but important differences emerge in specific places that have not previously been traversed by reflection/refraction profiles. The density of surface wave paths that are used in the analysis of Ren et al. (2013) implies that all parts of the model are subject to constraints on the velocity variation that are comparable in quality and objectivity, though horizontal resolution decreases with depth. Their images show clearly the areal extent of the region affected by the failed Tisza rift in the upper 5 to 10 km, and also suggest that reduced crustal thickness occurs in a diffuse band that crosses the basin beneath the MHZ.

The free-air gravity field across the basin (Fig. 1) clearly shows a trough aligned with the MHZ, supporting the crustal-scale nature of this feature. High free-air gravity anomalies associated with the Trans-Danubian ranges, the Carpathians and isolated regions like the Bükk Mountains (NE Hungary) are generally consistent with isostatically compensated crustal roots, which are clearly seen in the lows of the Bouguer gravity map (Bielik et al., 2006). Detailed modelling of specific transects shows, however, that the extent of this crustal root is variable; no root is evident beneath the West Carpathians, whereas strongly negative Bouguer anomalies along the South Carpathians require a significant crustal root to have developed (Szafián and Horváth, 2006).

In the present study we analyse the converted waves (P to S) from teleseismic signals recorded on a temporary broadband seismic array that spanned the western Pannonian Basin, in order to detect and measure Moho depth variation within the basin. The Carpathian Basins Project (CBP) (Dando et al., 2011; Hetényi et al., 2009) array comprised three lines of sensors separated by about 35 km each that covered a 75-km wide swath across Hungary, extending into eastern Austria and the northern part of Serbia. We use teleseismic signals recorded during the period April 2006 to August 2007. Our primary aim is to look for differences between the seismic signatures of the crust in the AlCaPa and Tisza terrains and, in particular, to describe the variation of crustal thickness across the basin. Of particular interest is the nature of the terrain boundary defined by the Mid-Hungarian shear zone.

2. Seismological data and receiver function processing

We analysed teleseismic records from the 46 broadband stations of the CBP array that were aligned in three NW–SE profiles spanning

from the Vienna Basin to the south-central part of the Pannonian Basin (see lines 2, 3 and 4 on Fig. 1). In addition, we also gathered data from permanent stations CONA (Austria), ZST (Slovakia), SOP and PKSM (Hungary), as well as other temporary stations installed as part of the CBP project: FGS (Serbia), and TIH (Hungary), for the same time period. Altogether, 284 teleseismic events of $M \geq 5.5$ provided 10,908 three component records for receiver function (RF) calculations. Hypocentral data for these events were obtained via the NEIC catalogue.

The quality of the data bears the signature of the sedimentary basin: relatively high background noise that sometimes masks the converted phases from distant and smaller magnitude events. To select the best quality data, we visually calibrate an automated quality control (QC) procedure in two steps:

1. The original ZNE-component data are band-pass filtered between 0.033 and 1 Hz frequency. Selected event data must meet three criteria:
   a) The root-mean-square (*rms*) amplitude of the signal computed between 30 s before and 120 s after the *P*-wave arrival has to be within 1 order of magnitude of the median of all *rms* values for the same event.
   b) The maximum amplitude of the main *P*-wave peak has to be at least 1.5 times higher than the maximum amplitude, and at least 3 times higher than the *rms* amplitude, of the preceding 20 s background on the Z-component for each trace.

These criteria confirm the impulsiveness of the *P*-wave in the data used to produce receiver functions. In our dataset 7770 traces (71% of the initial selection) have passed these QC criteria.

2. The original ZNE-component data are rotated to ZRT-components following the theoretical back-azimuth of the ray path. Then the radial component is de-convolved from the vertical component using the time-domain iterative approach of Ligorría and Ammon (1999) and using 90 iterations. The obtained series of spikes are then convolved with a Gaussian of width corresponding to the signal's highest frequency (1 Hz) to obtain the final radial receiver functions (RFs). To be utilised any RF must have the time of its maximum value within the range −1.2 to 2.2 s relative to the theoretical zero-time, and its amplitude a positive value not exceeding 0.8. After this test, 2960 traces are kept (38% of the initial selection).

To further improve the quality of the data used for imaging we exclude RFs obtained from teleseismic events of magnitude $M < 5.7$ and exclude aftershocks as sources, as their incoming *P*-waves interfere with the coda of the main shock, thus keeping 2034 good quality traces. We show in Fig. 2 stacked RFs for events sorted in back-azimuthal bins of width 20° for a selection of stations in different regions (locations indicated in Fig. 1). These stacks show variation of RFs with azimuth and give an indication of the quality of the signal relative to background noise. Similar diagrams for all stations used here are provided in the Supplementary Information file.

The final set of selected traces is then migrated using the common conversion point approach (Zhu, 2000). We use the 3D *P*-wave velocity model from the regional tomographic work of Piromallo and Morelli (2003) to convert the RF time series into depth, and use the V_P/V_S ratio of the *ak135* velocity model (Kennett et al., 1995) at each depth to create a 3D *S*-wave velocity model. We take into account the altitude of the stations and add another correction term (a shift of the RF trace) for the variable-thickness sediments. For this correction the depth of the basin is read from the map of Kilényi and Šefara (1989) beneath each station and local V_P value for the sediments is taken from Środa et al. (2006) with V_P/V_S of 2. The migration is performed on a grid aligned with the station array. Three 36-km wide swaths are defined with a bin size of 1 km * 1 km in the horizontal and vertical directions. Migrated images are constructed from events within 20°-wide back-azimuth bins and the normalised images from all back-azimuth bins are then averaged in order to avoid a preponderance of events from a given region dominating the final image. The final migrated cross-sections for each swath are presented both without and with smoothing (Fig. 3).

3. Technical limitations

An inherent difficulty for the analysis of this dataset is its location in a sedimentary basin: the basin has a highly variable basement topography which causes reverberations and a generally high background noise level. Another limitation of the RF calculation is the automated processing of the signals: despite a visual calibration of the selection criteria, the traces are not all visually verified. A limitation of the velocity model is its relatively sparse spatial definition (every 50 km) compared to the inter-station distance of the seismic array (ca. 35 km). A limitation of the migration scheme is that it presumes a single ray path along which the time-samples are distributed to form a depth image. We do not use multiples (*PpPmS* and *PpSmS* + *PsPmS* phases) to construct this image because we observe that in the Pannonian Basin strong variation of both the thickness and the wave-speed in the sediments leads to two artefacts. First, the correction term for the sediment depth uses the information beneath the station only once, and does not account for additional traverses through the sediment by the multiple phases (which are different for all traces). Second and more important: due to the strong velocity contrast between the sediments and the basement, underside reflections from the bottom of the sediments are present. These cause high-amplitude multiple phases that arrive earlier and appear shallower on the migrated image than normal multiples. Therefore our attempts to pick the *PpPmS* phase on an adapted migrated image and to determine average V_P/V_S ratios along the three profiles remain unsatisfactory. Although the general shape of the Moho is similar between the images obtained using multiples and those that use the direct conversion (*Ps* phase) only, the quantitative depth information that multiples provide remains unreliable in most cases here.

4. Results and interpretation

Fig. 3 shows a clear Moho of both the AlCaPa and Tisza units in all three profiles. Some interference with multiple conversions from the sedimentary base is visible, particularly for the southern ends of profiles 2 and 3 where sediments are thickest and near-surface crustal velocities slowest (Ren et al., 2013). The converted waves imaging the Moho have high amplitude in the central parts and somewhat weaker amplitudes in the NW end of the profiles. The SE ends of the profiles do not exhibit a clear and continuous Moho signature; the clear phase seen at the SE end of profile 3 emerges beneath a basement high (Fruska Gora, FGS, in Serbia) but it cannot be confidently connected to the other Moho picks of the Tisza unit. The RF Moho depths picked from Fig. 3 are used to

Fig. 1. Top: Topographic map of the Pannonian Basin region showing the surrounding mountain ranges and the two intra-Carpathian terrains, AlCaPa and Tisza, separated by the Mid-Hungarian Zone (MHZ), itself delimited by the Balaton Fault (BF) and the Mid-Hungarian Fault (MHF). Symbols show seismological stations (yellow: CBP profiles 2, 3 and 4; blue: additional CBP stations; red: permanent broadband stations), and piercing points of teleseismic rays used in this study at 33 km depth (orange). Profile definitions: zero distance on the middle profile (CBP3x) is at 46.92°N, 17.9°E and the profile is oriented at 140.5° clockwise from North. Profiles CBP2x and CBP4x are parallel to profile CBP3x and separated by 36 km to the NE (50.5°N) and resp. SW (230.5°N). Black dots mark the zero-distance points on each line, and every 50 km along profile CBP3x. Bottom: free-air gravity anomaly according to the EGM2008 model (Pavlis et al., 2012). A Gaussian filter of 20 km width has been applied to these data. The locations of three CBP profiles are repeated. The solid grey line marks the trace of the CEL08 active seismic line (see text).

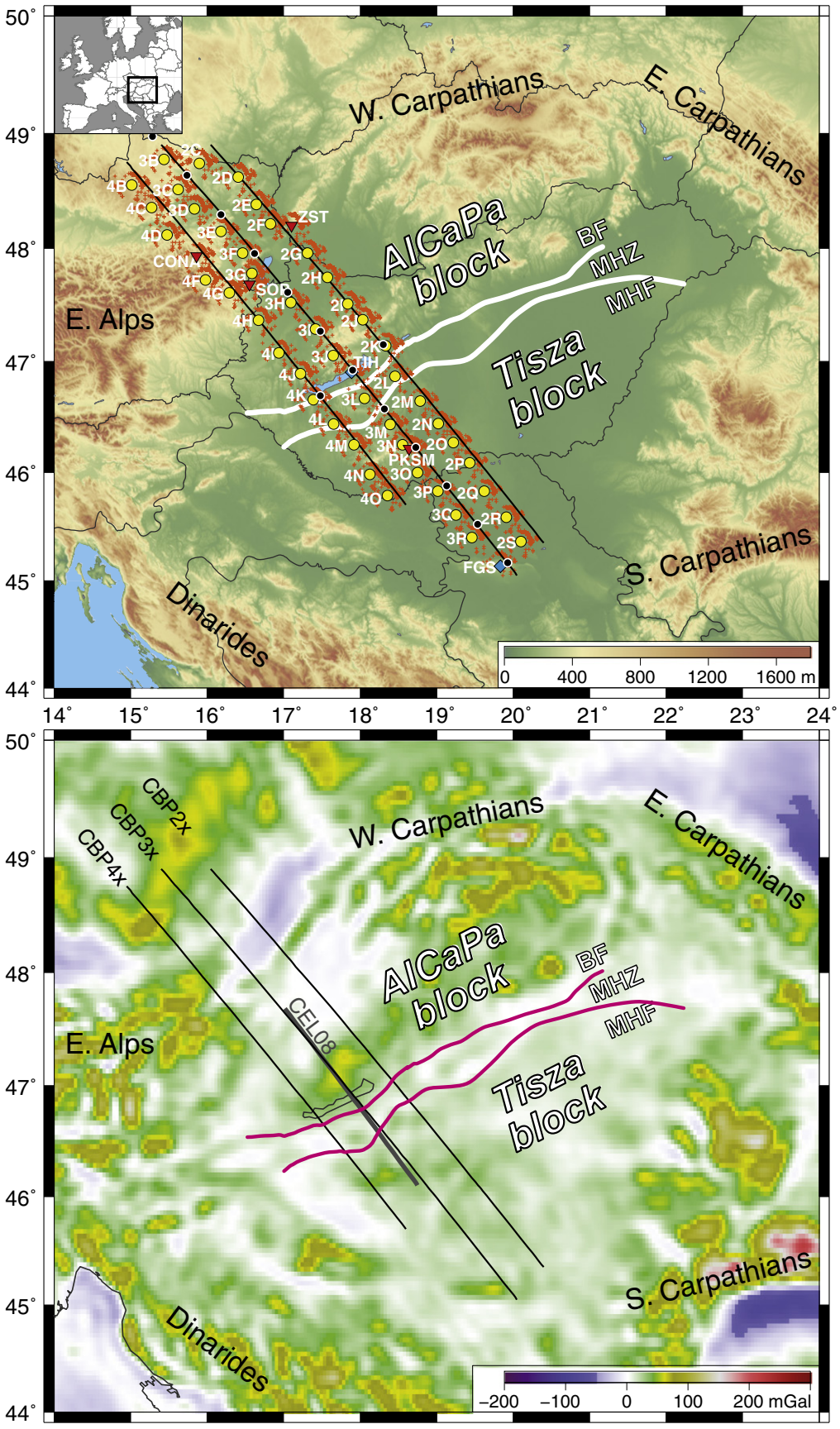
W. Carpathians
E. Carpathians
AlCaPa block
Tisza block
BF
MHZ
MHF
E. Alps
Dinarides
S. Carpathians
ZST
SOP
TIH
PKSM
FGS
0 400 800 1200 1600 m
CBP2x
CBP3x
CBP4x
CEL08
−200 −100 0 100 200 mGal
50°
49°
48°
47°
46°
45°
44°
14° 15° 16° 17° 18° 19° 20° 21° 22° 23° 24°

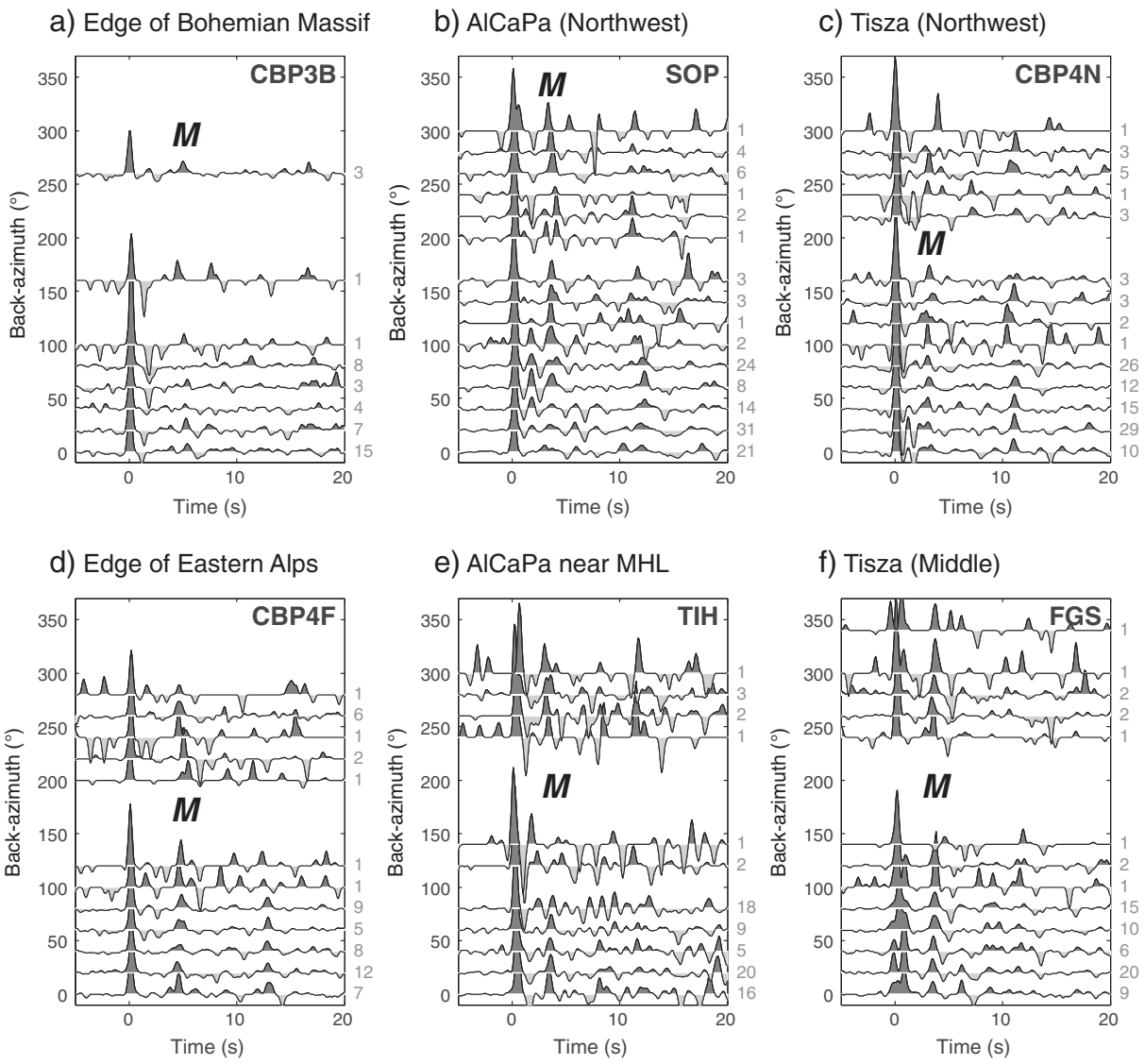

Fig. 2. Receiver function stacks for selected events at six stations at different geographic and tectonic locations (see Fig. 1). Records have been selected as described in the text and stacked in 20° wide back-azimuth bins. The numbers on the right of each frame indicate the number of traces that contribute to a stack. Letter "M" denotes the wave converted from P to S while crossing the Moho.

produce an interpolated map of Moho depth along a ca. 450 km * 75 km swath in Fig. 4. This diagram also shows the impact of lateral smoothing on the estimated Moho depths; the smoothed and unsmoothed images are similar, with the largest difference that Moho depths NW of the Trans-Danubian Ranges are 2–3 km deeper in the unsmoothed version of the map.

The Moho beneath the Pannonian Basin generally lies at depths of 25–30 km, with the shallowest regions near the centre of the basin, on either side of the MHZ. Fig. 4 shows the Moho at around 30 km depth beneath the MHZ, but this estimate is interpolated as there is no clear Moho signal in this region, as shown on the profiles (Fig. 3). Toward the perimeter of the basin, Moho depths increase to 30–35 km, and in the NW to depths of 45 km as the Alps are approached, as has been shown by Brückl et al. (2007) and Behm et al. (2007). Fig. 4 suggests also minor thickening of the crust toward the SW, but certainly minor compared to Moho thicknesses of between 40 and 55 km in the Dinarides determined by Stipčević et al. (2011) and Šumanovac et al. (2009). The Moho depths within the Pannonian Basin are in general agreement with prior receiver function studies (Bus, 2003; Hetényi and Bus, 2007), velocity models determined from local seismicity (Gráczer and Wéber, 2012) and numerous controlled source studies summarised by Grad et al. (2009).

The diffuse boundary between the main tectonic units AlCaPa and Tisza is marked by the Balaton and Mid-Hungarian Faults which occur between 0 and 50 km horizontal distance on our profiles (Figs. 1, 3, 5). These faults bound the sheared Mid-Hungarian Zone. The migrated RF profiles show the same Moho depth on either side of this narrow zone, within the uncertainty of our depth migration. This observation suggests that the two tectonic units, even if they have had different original crustal thickness, have thinned to the same final state. Although extension factors are locally variable and gravity anomalies suggest short wavelength depth variation of the Moho (Tari et al., 1999) the

Fig. 3. Migrated P-to-S receiver function cross-sections along lines 2, 3 and 4 of the CBP experiment. The top three plots (a) show the raw, unsmoothed version, and the bottom three (b) show the smoothed version (8 km horizontal Gaussian smoothing). The amplitude scale is +/−0.5 and +/−0.3%, respectively. Green ellipses mark the best pick for the Moho. Green dotted lines show the interpreted Moho for the AlCaPa and Tisza units. BF: Balaton Fault. MHZ: Mid-Hungarian Zone. MHF: Mid-Hungarian Fault. The zero coordinates on the horizontal axes are aligned with station TIH (black dots on Fig. 1).

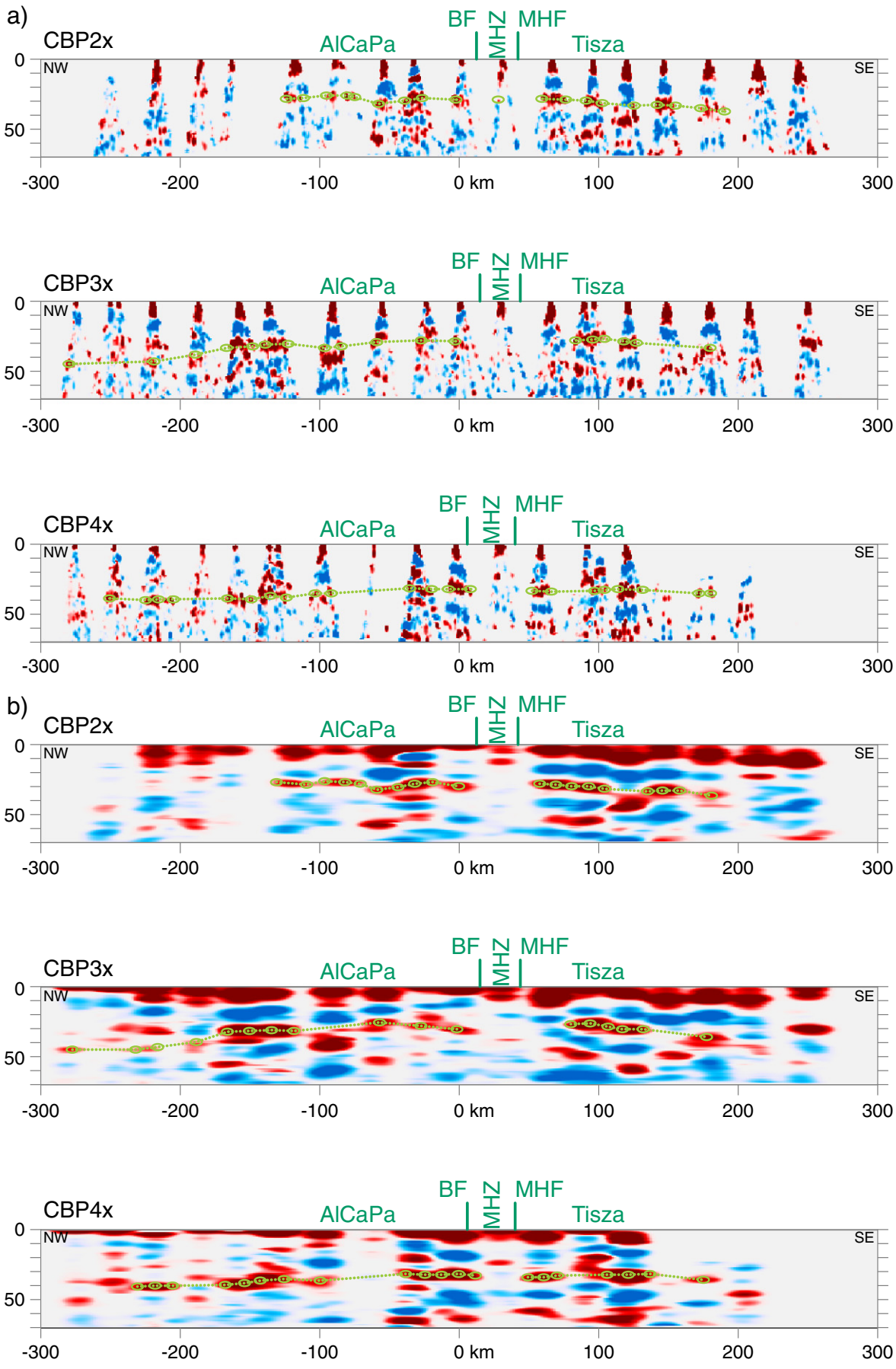
a)
CBP2x
AlCaPa
BF
MHZ
MHF
Tisza
NW
SE
0
50
-300
-200
-100
0 km
100
200
300
CBP3x
CBP4x
b)

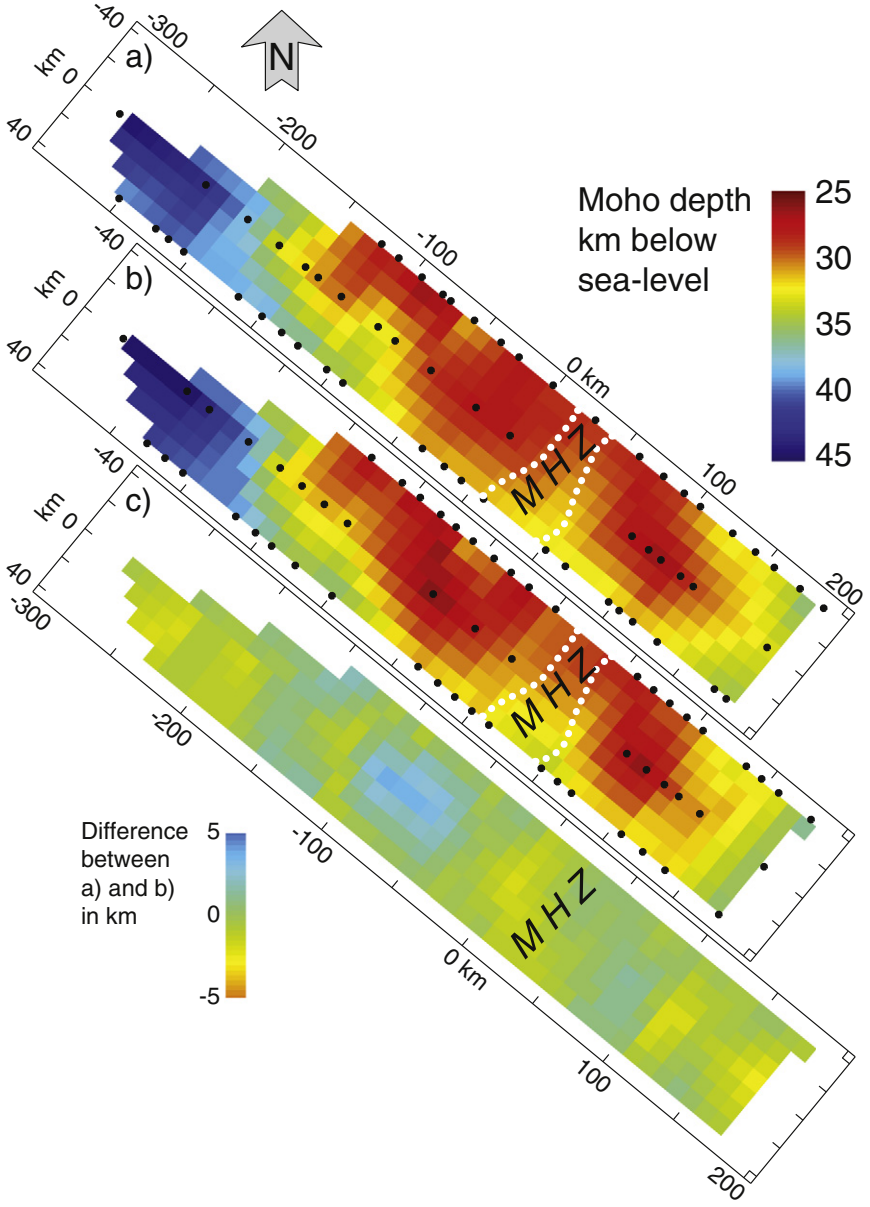

Fig. 4. Interpolated Moho map over a swath covering the 3 profiles: using the raw, non-smoothed images (a), and using the smoothed images (b). Black dots mark the location of Moho depth picks along the profiles. (c) The difference (a–b) of the two Moho maps shows the maximum artefact introduced by picking smoothed Moho depths (maximum difference is 3.5 km). The Mid-Hungarian Zone's location is shown (MHZ), together with the location of the BF and the MHF (white dotted lines). The cell size of these maps is 10 km * 10 km.

similarity of average crustal thickness in both AlCaPa and Tisza blocks implies that both have reached a similar mechanical equilibrium enabled by the mobilising effect of high heat flow through the Pannonian Basin crust.

Our migrated sections show no clear Moho conversion between the BF and the MHF. Unfortunately, however, the RFs obtained at the relevant stations (CBP2L, CBP3L and CBP4L) are few and of poor quality owing to reverberation of the signal in the sedimentary layer. Therefore, while the ca. 40 km wide Mid-Hungarian Zone, pinched between the AlCaPa and Tisza blocks, may possess a crust-mantle transition that is more gradational than the blocks on either side, the Moho conversion may be hidden in these noisy signals. Apparently absent Moho conversion has also been interpreted at other continental tectonic boundaries, for example in Tibet between the Lhasa and Qiangtang blocks, on either side of a major suture zone, the Banggong–Nujiang Suture (Nábělek et al., 2009).

The most reasonable explanation for an apparent lack of P-to-S conversion at the Moho is a gradual transition of shear-wave velocities between the crust and the mantle over a relatively thick zone. Posgay et al. (2006) described seismic and mineralogical evidence that supports the interpretation of progressive retrograde metamorphism having occurred in the extended basement of the Tisza block. In general these reactions are limited by the availability of crustal fluids. If the MHZ represents a zone of enhanced permeability, we tentatively suggest that a gradational Moho could be caused by serpentinisation of the uppermost mantle. Serpentinisation can be put in evidence only in very high quality seismic reflection surveys, but such data are not available at the MHZ. Alternatively, localized strike-slip shear on the MHZ also may have caused a depth-dependent reduction of upper mantle velocities in this region.

A subtle trough in both Bouguer (Kiss, 2009a; Tari et al., 1999) and free-air gravity anomalies coincides with the MHZ (Figs. 1, 5). About half of this gravity low (i.e., ca. 10–20 mGal in Bouguer anomalies) is

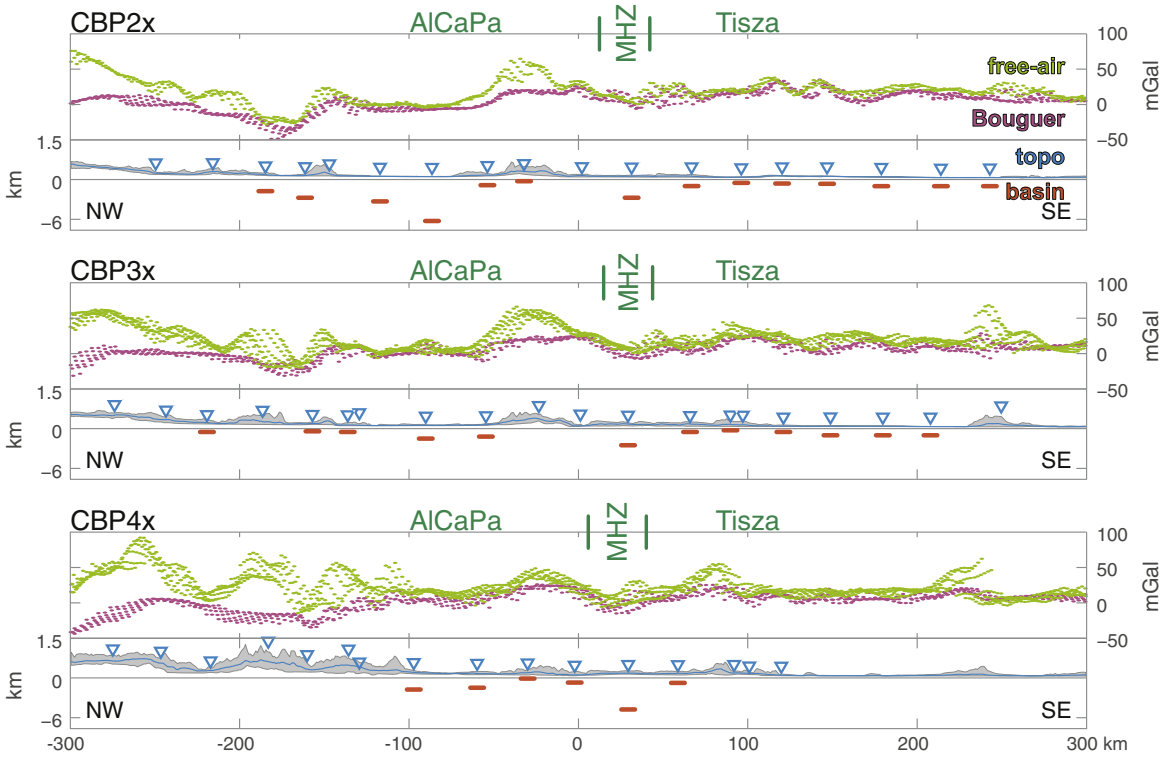

Fig. 5. Geophysical measurements along the three CBP profiles. Basin-depth (orange bars, from Kilényi and Šefara (1989), note 4-fold vertical compression compared to topography scale); topography (mean in blue, minimum–maximum range shaded in grey); free-air gravity anomalies in green (from EGM2008, Pavlis et al., 2012); and Bouguer anomalies in pink (from Tari et al., 1999). Scatter of gravity values is due to the 36 km width of each swath. Blue triangles mark the position of broadband seismological stations used in this study. MHZ: Mid-Hungarian Zone. Note the shallow relative lows in both gravity and topography corresponding to the MHZ.

likely to be explained by the relatively deeper basin (ca. 1000–1500 m on the map of Kilényi and Šefara, 1989) with thicker low-density sediments along the MHZ. If Moho depth variation also contributes to this gravity low, then we would expect the Moho to be locally deeper in addition to its being more gradational in depth beneath the MHZ. Other seismic data contradict this idea (see next section), but a shallower Moho with serpentinised upper mantle might also contribute to a negative gravity anomaly beneath the MHZ. SE of the MHZ, variations in Bouguer gravity are short wavelength and low amplitude, consistent with the idea that Moho depth is relatively constant across the Tisza block. NW of the MHZ, a clearly defined gradient in the Bouguer anomaly is consistent with the increasing Moho depth toward the Alps.

5. Comparison to prior studies of seismic structure

We now compare our receiver function profiles to other seismic measurements for the same region.

The seismic refraction line CEL08 was acquired in the frame of the CELEBRATION (Central European Lithospheric Experiment Based on Refraction 2000) campaign (Guterch et al., 2003). The interpretation

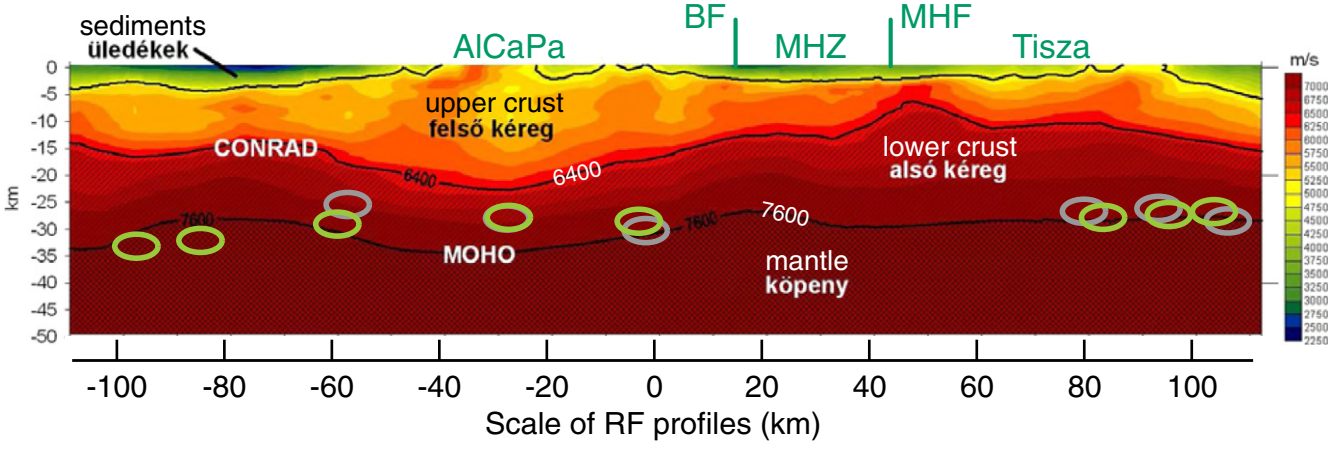

Fig. 6. Comparison of RF Moho depth picks from Fig. 3 (CBP3x ellipses, green: raw image, grey: smoothed image) with seismic velocity section from the CEL08 line, as shown on Fig. 9 of Kiss (2009b). BF: Balaton Fault. MHZ: Mid-Hungarian Zone. MHF: Mid-Hungarian Fault.

of line CEL08 is published and thoroughly analysed by Kiss (2009b). CEL08 is very closely aligned with our receiver function profile CBP3x (Fig. 1). Fig. 6 shows the interpreted crustal structure and velocity section of Kiss (2009b), on top of which the migrated RF Moho depths are also shown. The match between the RF Moho depth and the crust-mantle boundary interpreted from refraction is generally consistent. In this comparison the RF Moho depth picks fall on or near the $V_P = 7600$ m/s velocity contour. Such a velocity value, intermediate between crust and mantle velocities, can reasonably define the Moho depth in a tomographic inversion which cannot resolve a sharp discontinuity. The refraction Moho is somewhat shallower beneath the MHZ, and the justification for a more gradational Moho in this region is no clearer. The CEL08 line also suggests a deeper Moho beneath the Trans-Danubian Ranges (at ca. −30 km distance on Fig. 6), which is not detected in the CBP3x profile, though there is some hint of a deeper Moho at the same distance on the CBP2x profile.

We also compare our RF Moho depth picks with shear-wave velocity sections taken from a recent tomographic inversion of crustal velocities determined from surface wave analysis (ambient noise correlation) by Ren et al. (2013). On the CBP2x and CBP3x profiles, the RF Moho picks generally are within the range $V_S = 3.7$–3.9 km/s (Fig. 7). The RF picks are less consistent and generally a little deeper than the $V_S = 3.9$ km/s contour on the south-western profile (CBP4x). Also shown on Fig. 7 are the corresponding Moho depth profiles extracted from the regional compilations of Tesauro et al. (2008) and Grad et al. (2009). All four datasets generally agree on Moho depth across most of the basin, but the two compilations do not show the Moho deepening to the SE, as is evident in both RF Moho depths and the V_S field from surface wave tomography. We assume that the regional compilations are less constrained by data from the northern part of Serbia.

The general similarity in crustal thickness between AlCaPa and Tisza blocks (Fig. 4) and the Miocene–Pliocene change from extension to contraction (Bada et al., 2007) in both regions suggests that both domains together reached a mechanical equilibrium between internal gravitational potential energy (determined mainly by crustal thickness) and externally derived horizontal stress. This type of equilibrium implies that both regions are weak compared to normal lithosphere, as suggested by Cloetingh et al. (2006) and differences in effective lithospheric strength that may be expected from their differing extension histories (Cloetingh et al., 2006) are not evident. The similarity in recent tectonic history of the two regions is also evident in the signature of anisotropy obtained from the fast polarization directions of SKS waves recorded at the CBP array (Fig. 5 of Kovács et al., 2012). These fast polarization directions are predominantly E–W on CBP3x and CBP4x lines, but several of the stations on CBP2x are closer to NW–SE on both of the crustal blocks. This variation may be related to the continuing convergence of the Adriatic block with Europe but, whatever the cause, both crustal blocks appear similarly affected. We might infer from both crustal thickness and seismic fabric that both AlCaPa and Tisza blocks have experienced a comparable recent strain field, and that the similarity of their present-day seismic signatures contrasts markedly with the signature of an earlier deformation phase in which paleomagnetic rotations of opposite sign left their imprint on the two blocks.

6. Conclusions

The Moho depths determined from the CBP receiver functions reveal a relatively simple pattern of crustal thinning which has affected both AlCaPa and Tisza blocks to a similar result. Crustal thickness across most of the western Pannonian Basin is in the range 25 to 30 km, gradually increasing toward the periphery of the basin, with maximum crustal thickness values of about 45 km observed near the Eastern Alps. At this scale the crustal layers of the two major blocks AlCaPa and Tisza appear structurally similar, from which we infer that the extent of crustal thinning was ultimately limited in both cases by an equilibrium, enabled by the high heat flow of the basin, between internal gravitational forces

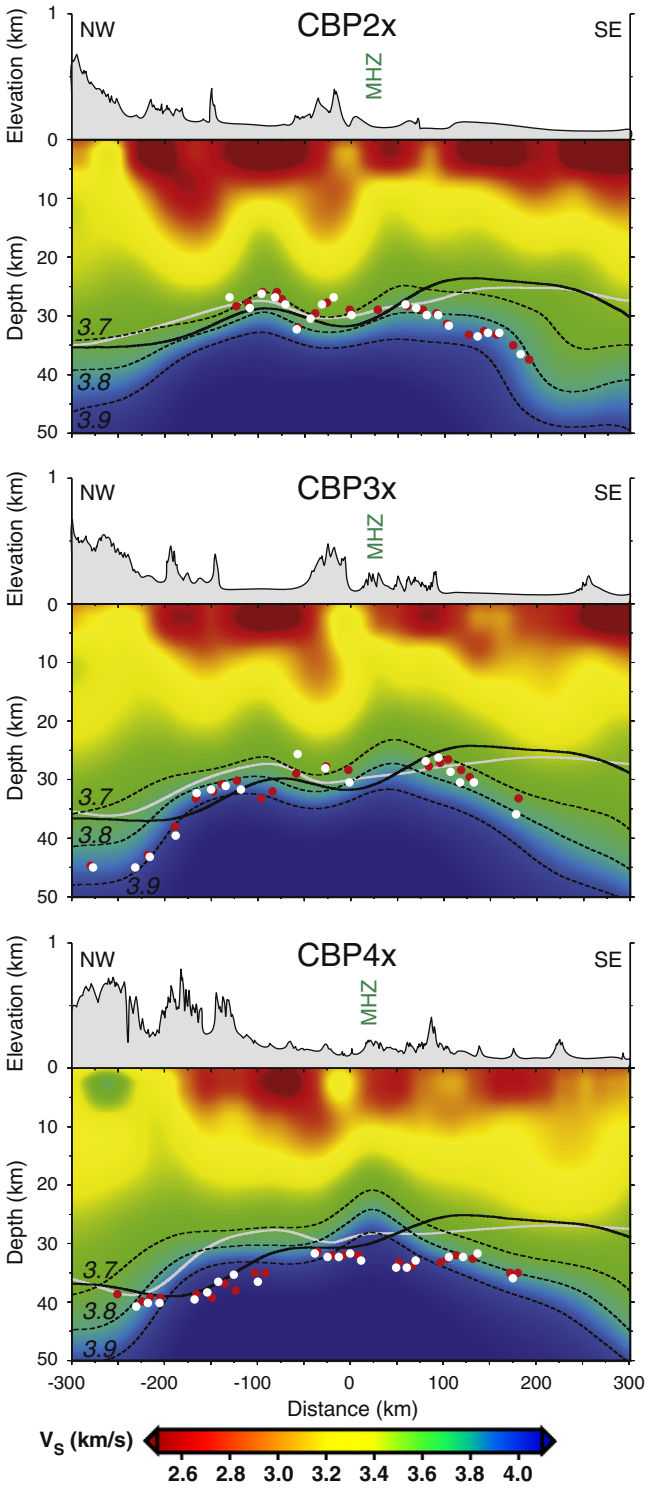

Fig. 7. Comparison of receiver function Moho depth picks with V_S profiles from ambient noise tomography of Ren et al. (2013). Red and white circles correspond to Moho depth picks from Fig. 3 on unsmoothed and smoothed RF migrated images, respectively. Dashed lines are the 3.7, 3.8 and 3.9 km/s iso-velocity contours of the 3D V_S field obtained by tomographic inversion of surface waves extracted from cross-correlation of ambient seismic noise. The grey and black continuous lines correspond to Moho depths interpolated from the models of Tesauro et al. (2008) and Grad et al. (2009), respectively. Note different vertical exaggeration factors on V_S sections and topographic profiles. MHZ: Mid-Hungarian Zone.

that depend mainly on crustal thickness and external constraining stress. In this context we note also that there is no clear contrast between the anisotropy signatures of AlCaPa and Tisza block. Both of these observations suggest that the recent tectonic history of the two neighbouring blocks is similar.

The Mid-Hungarian zone, whose role in the extension of the Pannonian Basin has long been fairly enigmatic, has not been clearly imaged in this study. A possible explanation for the lack of a clear Moho signal in this region is that the velocity change from crust to mantle is relatively gradational there. Taking into account earlier seismic studies which suggest that the Moho is shallower beneath the MHZ and that gravity is relatively low by 10 or 20 mGal along the MHZ, we speculate that the uppermost mantle beneath the MHZ is potentially serpentinised and the overlying crust in this region has been more strongly affected by retrograde metamorphism than the crust in the adjoining blocks. These metamorphic processes depend upon the availability of fluids which are likely to more easily infiltrate the highly strained crust of the MHZ.

Acknowledgements

CBP was supported by a NERC standard grant (NE/C004574/1). The NERC Geophysical Equipment Pool (SEIS-UK) provided most of the seismological equipment used in the CBP network. Eötvös Loránd Geophysical Institute (ELGI), Technical University of Vienna (TU Wien) and the Seismological Survey of Serbia (SSS) provided extensive logistical support for fieldwork. Additional data were provided by Geofon, the GFZ Seismological Data Archive, ORFEUS, IRIS and the Hungarian Academy of Sciences, Geodetical and Geophysical Research Institute. We thank Frank Horváth for comments on a draft manuscript, and Marek Grad and another anonymous reviewer for helpful suggestions which improved the presentation. Figs. 1 and 7 were produced using GMT (Wessel and Smith, 1998).

Appendix A. Supplementary data

Supplementary data to this article can be found online at http://dx.doi.org/10.1016/j.tecto.2015.02.004.

References

Bada, G., Horváth, F., Dövényi, P., Szafián, P., Windhoffer, G., Cloetingh, S., 2007. Present-day stress field and tectonic inversion in the Pannonian basin. Glob. Planet. Chang. 58, 165–180. http://dx.doi.org/10.1016/j.gloplacha.2007.01.007.

Behm, M., Brückl, E., Chwatal, W., Thybo, H., 2007. Application of stacking and inversion techniques to three-dimensional wide-angle reflection and refraction data of the Eastern Alps. Geophys. J. Int. 170, 275–298. http://dx.doi.org/10.1111/j.1365-246X.2007.03393.x.

Bielik, M., Kloska, K., Meurers, B., Svancara, J., Wybraniec, S., CELEBRATION 2000 Potential Field Working Group, 2006. Gravity anomaly map of the CELEBRATION 2000 region. Geol. Carpath. 57 (3), 145–156.

Brückl, E., et al., 2007. Crustal structure due to collisional and escape tectonics in the Eastern Alps region based on profiles Alp01 and Alp02 from the ALP 2002 seismic experiment. J. Geophys. Res. 112, B06308. http://dx.doi.org/10.1029/2006JB004687.

Bus, Z., 2003. S-wave velocity structure beneath the Mátra Mountains (Hungary) inferred from teleseismic receiver functions. Acta Geod. Geophys. Hung. 38 (1), 93–102.

Cloetingh, S., Bada, G., Matenco, L., Lankreijer, A., Horváth, F., Dinu, C., 2006. Modes of basin (de)formation, lithospheric strength and vertical motions in the Pannonian–Carpathian system: inferences from thermo-mechanical modelling. In: Gee, D.G., Stephenson, R.A. (Eds.), European Lithosphere Dynamics. Geological Society London, Memoir 32, pp. 207–221. http://dx.doi.org/10.1144/GSL.MEM.2006.032.01.12.

Csontos, L., Nagymarosy, A., 1998. The Mid-Hungarian line: a zone of repeated tectonic inversions. Tectonophysics 297, 51–71.

Csontos, L., Vörös, A., 2004. Mesozoic plate tectonic reconstruction of the Carpathian region. Paleogeogr. Paleoclimatol. Paleoecol. 210, 1–56. http://dx.doi.org/10.1016/j.palaeo.2004.02.033.

Csontos, L., Tari, G., Bergerat, F., Fodor, L., 1991. Evolution of the stress fields in the Carpatho-Pannonian area during the Neogene. Tectonophysics 199, 73–91.

Csontos, L., Nagymarosy, A., Horváth, F., Kovac, M., 1992. Tertiary evolution of the Intra-Carpathian area: a model. Tectonophysics 208, 221–241.

Csontos, L., Marton, E., Worum, G., Benkovics, L., 2002. Geodynamics of SW-Pannonian inselbergs (Mecsek and Villany Mts, SW Hungary). EGU Stefan Mueller Spec. Publ. Ser. 3, 227–245.

Dando, B.D.E., Stuart, G.W., Houseman, G.A., Hegedus, E., Bruckl, E., Radovanovic, S., 2011. Teleseismic tomography of the mantle in the Carpathian–Pannonian region of central Europe. Geophys. J. Int. 186, 11–31. http://dx.doi.org/10.1111/j.1365-246X.2011.04998.x.

Gemmer, L., Houseman, G.A., 2007. Convergence and extension driven by lithospheric gravitational instability: evolution of the Alpine–Carpathian–Pannonian system. Geophys. J. Int. 168 (3), 1276–1290. http://dx.doi.org/10.1111/j.1365-246X.2006.03327.x.

Grácz, Z., Wéber, Z., 2012. One-dimensional P-wave velocity model for the territory of Hungary from local earthquake data. Acta Geod. Geophys. Hung. 47 (3), 344–357. http://dx.doi.org/10.1556/AGeod.47.2012.3.5.

Grad, M., Guterch, A., Keller, G.R., Janik, T., Hegedus, E., Vozar, J., Slaczka, A., Tiira, T., Yliniemi, J., 2006. Lithospheric structure beneath trans-Carpathian transect from Precambrian platform to Pannonian basin: CELEBRATION 2000 seismic profile CEL05. J. Geophys. Res. 111, B03301. http://dx.doi.org/10.1029/2005JB003647.

Grad, M., Tiira, T., ESC Working Group, 2009. The Moho depth map of the European plate. Geophys. J. Int. 176, 279–292.

Guterch, A., Grad, M., Keller, G.R., Posgay, K., Vozár, J., Špičák, A., Brückl, E., Hajnal, Z., Thybo, H., Selvi, O., CELEBRATION 2000 experiment team, 2003. CELEBRATION 2000 seismic experiment. Stud. Geophys. Geod. 47, 659–669.

Hetényi, G., Bus, Z., 2007. Shear wave velocity and crustal thickness in the Pannonian Basin from receiver function inversions at four permanent stations in Hungary. J. Seismol. 11, 405–414. http://dx.doi.org/10.1007/s10950-007-9060-4.

Hetényi, G., Stuart, G.W., Houseman, G.A., Horváth, F., Hegedus, E., Brückl, E., 2009. Anomalously deep mantle transition zone below Central Europe: evidence of lithospheric instability. Geophys. Res. Lett. 36, L21307. http://dx.doi.org/10.1029/2009GL040171.

Horváth, F., 1993. Towards a mechanical model for the formation of the Pannonian Basin. Tectonophysics 226, 333–357.

Horváth, F., Dövényi, P., Szalay, Á., Royden, L.H., 1988. Subsidence, thermal and maturation history of the Great Hungarian Plain. In: Royden, L.H., Horváth, F. (Eds.), The Pannonian Basin: a Study in Basin Evolution. American Association of Petroleum Geologists, Memoir 45, pp. 355–372.

Horváth, F., Bada, G., Szafian, P., Tari, G., Adam, A., Cloetingh, S., 2006. Formation and deformation of the Pannonian Basin: constraints from observational data. In: Gee, D.G., Stephenson, R.A. (Eds.), European Lithosphere Dynamics. Geological Society London, Memoir 32, pp. 191–206. http://dx.doi.org/10.1144/GSL.MEM.2006.032.01.11.

Kennett, B.L.N., Engdahl, E.R., Buland, R., 1995. Constraints on seismic velocities in the Earth from traveltimes. Geophys. J. Int. 122, 108–124.

Kilényi, É., Šefara, J. (Eds.), 1989. Pre-Tertiary Basement Contour Map of the Carpathian Basin Beneath Austria, Czechoslovakia and Hungary. 1: 500,000. ELGI, Budapest.

Kiss, J., 2009a. Regionális gravitációs anomáliák, izosztatikus hatások Magyarországon. Magy. Geofiz. 50 (4), 153–171.

Kiss, J., 2009b. A CEL08 szelvény geofizikai vizsgálata. Magy. Geofiz. 50 (2), 59–74.

Kovács, I., Csontos, L., Szabó, Cs, Bali, E., Falus, Gy, Benedek, K., Zajacz, Z., 2007. Paleogene–early Miocene igneous rocks and geodynamics of the Alpine–Carpathian–Pannonian–Dinaric region: an integrated approach. In: Beccaluva, L., Bianchini, G., Wilson, M. (Eds.), Cenozoic Volcanism in the Mediterranean Area. Geol. Soc. Am. Spec. Pap 418, pp. 93–112. http://dx.doi.org/10.1130/2007.2418(05).

Kovács, I., Falus, Gy, Stuart, G., Hidas, K., Szabó, Cs, Flower, M., Hegedűs, E., Posgay, K., Zilahi-Sebess, L., 2012. Seismic anisotropy and deformation patterns in upper mantle xenoliths from the central Carpathian–Pannonian region: asthenospheric flow as a driving force for Cenozoic extension and extrusion? Tectonophysics 514–517, 168–179. http://dx.doi.org/10.1016/j.tecto.2011.10.022.

Ligorría, J.P., Ammon, C.J., 1999. Iterative deconvolution and receiver-function estimation. Bull. Seismol. Soc. Am. 89, 1395–1400.

Lorinczi, P., Houseman, G.A., 2010. Geodynamical models of lithospheric deformation, rotation and extension of the Pannonian Basin of Central Europe. Tectonophysics 492, 73–87.

Nábělek, J., Hetényi, G., Vergne, J., et al., 2009. Underplating in the Himalaya–Tibet collision zone revealed by the Hi-CLIMB experiment. Science 325 (5946), 1371–1374.

Patrascu, S., Panaiotu, C., Seclaman, M., Panaiotu, C.E., 1994. Timing of rotational motion of Apuseni Mountains (Romania): paleomagnetic data from Tertiary magmatic rocks. Tectonophysics 233, 163–176.

Pavlis, N.K., Holmes, S.A., Kenyon, S.C., Factor, J.K., 2012. The development and evaluation of the Earth Gravitational Model 2008 (EGM2008). J. Geophys. Res. 117 (B4). http://dx.doi.org/10.1029/2011JB008916.

Piromallo, C., Morelli, A., 2003. P wave tomography of the mantle under the Alpine–Mediterranean area. J. Geophys. Res. 108 (B2), 2065. http://dx.doi.org/10.1029/2002JB001757.

Posgay, K., Bodoky, T., Hajnal, Z., Toth, T.M., Fancsik, T., Hegedus, E., Kovacs, A.C., Takacs, E., 2006. Interpretation of subhorizontal crustal reflections by metamorphic and rheologic effects in the eastern part of the Pannonian Basin. Geophys. J. Int. 167, 187–203.

Ren, Y., Grecu, S., Stuart, G., Houseman, G., Hegedus, E., South Carpathian Working Group, 2013. Crustal structure of the Carpathian–Pannonian region from ambient noise tomography. Geophys. J. Int. http://dx.doi.org/10.1093/gji/ggt316.

Schmid, S.M., Bernoulli, D., Fügenschuh, B., Matenco, L., Scheffer, S., Schuster, R., Tischler, M., Ustaszewski, K., 2008. The Alpine–Carpathian–Dinaridic orogenic system: correlation and evolution of tectonic units. Swiss J. Geosci. 101, 139–183. http://dx.doi.org/10.1007/s00015-008-1247-3.

Sclater, J.G., Royden, L., Horváth, F., Burchfiel, B.C., Semken, S., Stegena, L., 1980. The formation of the Intra-Carpathian basins as determined from subsidence data. Earth Planet. Sci. Lett. 51, 139–162.

Środa, P., Czuba, W., Grad, M., Guterch, A., Tokarski, A.K., Janik, T., Rauch, M., Keller, G.R., Hegedűs, E., Vozár, J., CELEBRATION 2000 Working Group, 2006. Crustal and upper

mantle structure of the Western Carpathians from CELEBRATION 2000 profiles CEL01 and CEL04: seismic models and geological implications. Geophys. J. Int. 167, 737–760. http://dx.doi.org/10.1111/j.1365-246X.2006.03104.x.

Stegena, L., Géczy, B., Horváth, F., 1975. Late Cenozoic evolution of the Pannonian Basin. Tectonophysics 26, 71–90.

Stipčević, J., Tkalčić, H., Herak, M., Markušić, S., Herak, D., 2011. Crustal and uppermost mantle structure beneath the External Dinarides, Croatia, determined from teleseismic receiver functions. Geophys. J. Int. 185, 1103–1119. http://dx.doi.org/10.1111/j.1365-246X.2011.05004.x.

Šumanovac, F., Orešković, J., Grad, M., ALP 2002 Working Group, 2009. Crustal structure at the contact of the Dinarides and Pannonian basin based on 2-D seismic and gravity interpretation of the Alp07 profile in the ALP 2002 experiment. Geophys. J. Int. 179, 615–633. http://dx.doi.org/10.1111/j.1365-246X.2009.04288.x.

Szafián, P., Horváth, F., 2006. Crustal structure in the Carpath-Pannonian region: insights from three-dimensional gravity modelling and their geodynamic significance. Int. J. Earth Sci. (Geol. Rundsch.) 95, 50–67.

Tari, G., Horváth, F., Rumpler, J., 1992. Styles of extension in the Pannonian Basin. Tectonophysics 208, 203–219.

Tari, G., Dövényi, P., Dunkl, I., Horváth, F., Lenkey, L., Stefanescu, M., Szafián, P., Tóth, T., 1999. Lithospheric structure of the Pannonian basin derived from seismic, gravity and geothermal data. Geol. Soc. Lond. Spec. Publ. 156, 215–250. http://dx.doi.org/10.1144/GSL.SP.1999.156.01.12.

Tesauro, M., Kaban, M.K., Cloetingh, S.A.P.L., 2008. EuCRUST-07: a new reference model for the European crust. Geophys. Res. Lett. 35, L05313. http://dx.doi.org/10.1029/2007GL032244.

Ustaszewski, K., Schmid, S.M., Fugenschuh, B., Tischler, M., Kissling, E., Spakman, W., 2008. A map-view restoration of the Alpine–Carpathian–Dinaridic system for the Early Miocene. Swiss J. Geosci. 101 (Suppl. 1), S273–S294.

Wessel, P., Smith, W.H.F., 1998. New, improved version of the Generic Mapping Tools released. EOS Trans. AGU 79, 579.

Zhu, L.P., 2000. Crustal structure across the San Andreas Fault, southern California from teleseismic converted waves. Earth Planet. Sci. Lett. 179, 183–190. http://dx.doi.org/10.1016/S0012-821X(00)00101-1.